

# Border extrapolation using fractal attributes in remote sensing images

M.P. Cipolletti<sup>a,\*</sup>, C.A. Delrieux<sup>a,\*\*</sup>, G.M.E. Perillo<sup>b,c</sup>, M.C. Piccolo<sup>b,d</sup>

<sup>a</sup> Instituto de Investigaciones en Ingeniería Eléctrica and Dpto. de Ing. Eléctrica y de Computadoras, Universidad Nacional del Sur (UNS) – Consejo Nacional de Investigaciones Científicas y Tecnológicas (CONICET) Bahía Blanca, Argentina

<sup>b</sup> Instituto Argentino de Oceanografía, CONICET, Bahía Blanca, Argentina

<sup>c</sup> Departamento de Geología, UNS, Bahía Blanca, Argentina

<sup>d</sup> Departamento de Geografía y Turismo, UNS, Bahía Blanca, Argentina

## ARTICLE INFO

### Article history:

Received 13 December 2012

Received in revised form

2 August 2013

Accepted 9 September 2013

Available online 21 September 2013

### Keywords:

Perimeter

Extrapolation

Richardson

Fractal dimension

## ABSTRACT

In management, monitoring and rational use of natural resources the knowledge of precise and updated information is essential. Satellite images have become an attractive option for quantitative data extraction and morphologic studies, assuring a wide coverage without exerting negative environmental influence over the study area. However, the precision of such practice is limited by the spatial resolution of the sensors and the additional processing algorithms. The use of high resolution imagery (i.e., Ikonos) is very expensive for studies involving large geographic areas or requiring long term monitoring, while the use of less expensive or freely available imagery poses a limit in the geographic accuracy and physical precision that may be obtained.

We developed a methodology for accurate border estimation that can be used for establishing high quality measurements with low resolution imagery. The method is based on the original theory by Richardson, taking advantage of the fractal nature of geographic features. The area of interest is downsampled at different scales and, at each scale, the border is segmented and measured. Finally, a regression of the dependence of the measured length with respect to scale is computed, which then allows for a precise extrapolation of the expected length at scales much finer than the originally available. The method is tested with both synthetic and satellite imagery, producing accurate results in both cases.

© 2013 Elsevier Ltd. All rights reserved.

## 1. Introduction

Geomorphologic and oceanographic studies based on the use of physical-numerical models require a precise knowledge of geographic magnitudes in order to be applied (areas, coastline lengths, etc.). These quantities are not always available because the geographic features in study are located in difficult access areas, involve large extensions or direct measuring itself generates a negative environmental effect or introduces modifications in the evolution of the observed system. In these cases, the analysis of morphologic features from satellite images is an advantageous alternative (Schowengerdt, 1997; Lillesand and Kiefer, 2000; Chen and Ho, 2008). While the use of coarse spatial resolution images limits the precision, the use of fine spatial resolution images

implies an excessive cost to cover large areas. Such situation motivates the development of reliable data-approximation techniques from coarse spatial resolution images.

Fractal geometry offers an ideal theoretical background to develop estimation algorithms. Its concepts and applications extend to all fields of human experience (Russ, 1993; Falconer, 2003) including natural sciences (Mandelbrot, 1983; Siu and Lam, 2002; Lopes and Betrouni, 2009). In digital image processing (DIP), fractal theory is the basis of several techniques for purposes such as segmentation, measurement, pattern recognition, etc. (Zhende and Yuwen, 2003; Lopes and Betrouni, 2009; García et al., 2010).

Richardson (1961), in his mathematical analysis of war, was the first to notice the relationship between geographic measurement and scale. In his work, measurement of borders between countries is performed by approximating the contour using a polygonal path composed of constant module segments  $\epsilon$  and, as  $\epsilon \rightarrow 0$ , Richardson infers that the result approaches a limit. In the case of coastlines, which are continuous but not necessarily derivable curves, an increment in resolution implies the appearance of finer and finer details in a way such that the total magnitude appears to diverge  $L(\epsilon) \rightarrow \infty$  (Fig. 1). As a consequence, the measured length of

\* Corresponding author. Current address: CC804, B8000FWB Bahía Blanca, Argentina. Tel.: +54 291 486 1112/1519/1309; fax: +54 291 486 1527/1112/1519.

\*\* Principal corresponding author.

E-mail addresses: [mpcipolletti@gmail.com](mailto:mpcipolletti@gmail.com) (M.P. Cipolletti), [cad@uns.edu.ar](mailto:cad@uns.edu.ar) (C.A. Delrieux), [gmeperillo@criba.edu.ar](mailto:gmeperillo@criba.edu.ar) (G.M.E. Perillo), [piccolo@criba.edu.ar](mailto:piccolo@criba.edu.ar) (M.C. Piccolo).

the border depends on the precision employed in the calculation and the final result increases for a higher level of detail. However, Richardson (1961) developed a function to estimate borders among countries, which is defined as

$$L(\epsilon) = F\epsilon^{1-D} \quad (1)$$

where  $F$  and  $D$  are characteristic constants of each contour. Mandelbrot (1967) followed the studies by Richardson and proposed to use the exponent  $D$  as a natural dimension, also called fractional dimension or fractal dimension (FD) which, in certain cases, coincides with the Hausdorff–Besicovitch dimension (Mandelbrot, 1983; Falconer, 2003).

The standard fractal analysis method is formulated by Richardson (Richardson, 1961; Mandelbrot, 1967; Dutch, 1993) where the invariance to scale is established in the  $\log(\text{Length}) - \log(\text{Scale})$  plane. Nevertheless, different authors present FD measurement algorithms and analyze their performance (Allen et al., 1995; Soille and Rivest, 1996; Schlueter et al., 1997; Dillon et al., 2001; Lopes and Betrouni, 2009). In particular, for feature and texture characterization, the approaches are mainly concerned with the accuracy of the algorithms (Allen et al., 1995; Soille and Rivest, 1996), the conditions to validate the results (Goodchild, 1980; Shelberg et al., 1982; Wu, 2004; Wu et al., 2006) or the description of pattern distribution (Korčák, 1938; Mandelbrot, 1983; Lipiec et al., 1998; Zuo et al., 2009; Imre et al., 2011). Also, simpler

techniques like the one proposed by Håkanson (1978) are only focusing on feature estimation.

Håkanson (1978) uses fractal analysis to estimate the perimeter of twelve lakes in Sweden. In his work, he claims that it is not possible to evaluate the precision of a measurement results without specifying the method used and establishing rules for selecting an adequate scale. He also develops an empiric expression of the length variation which allows to compare the different scales among the lakes. However, some authors question the reliability of his work due to the information incongruence in the calculations when using heterogeneous cartography (Mark and Aronson, 1984; Lam and Quattrochi, 1992). In DIP, the standard measurement algorithms or “chain codes” (Freeman, 1961, 1970; Dunkelberger and Mitchell, 1985) present a high degree of systematic associated error (Kulpa, 1983; Dorst and Smeulders, 1987; Yang et al., 1994; Imre, 2006; Cipolletti et al., 2012).

The purpose of this work is to further develop the fractal estimation techniques using consistent data sources and more accurate length measurement algorithms to apply them in satellite imagery. In this way, we are able to perform high quality border measurements with low resolution imagery. The proposed methodology is based on measuring the border at different scales and, then, computing a regression of the dependence of the measured length with respect to scale. This enables the extrapolation of precise length measures using imagery of coarse spatial resolution without the information incongruence problems present in Håkanson algorithm. The method was tested on synthetic images and on Landsat images of Buenos Aires Province (Argentina). In the latter case, the work focuses in coastal areas of the Bahía Blanca Estuary. In all the experiments, we were able to extract border measurements from coarse resolution images that are significantly similar to the values measured at much finer resolution.

## 2. Methodology

In satellite imagery, each pixel has color or radiance information divided into  $n$ -bands and an associated spatial-resolution value  $S$  corresponding to the pixel side length. Fig. 2 shows the length estimation process: segmentation + downsampling + border measurement + fractal regression. This method lets to predict the value of a measurement in a finer scale than that of the original image avoiding information incongruence problems caused by the use of heterogeneous cartography (Håkanson, 1978; Mark and Aronson, 1984; Lam and Quattrochi, 1992).

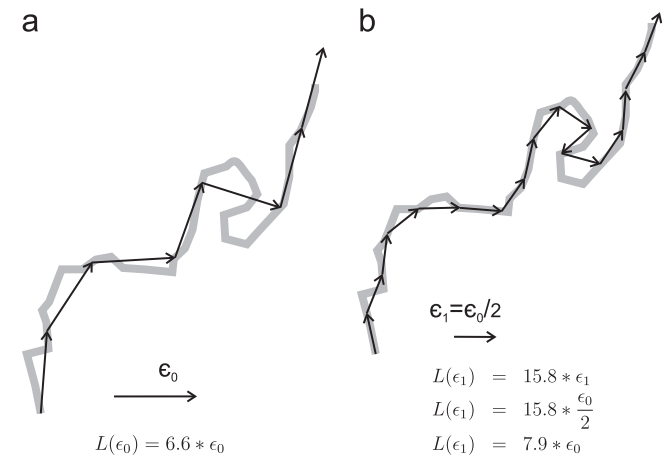


Fig. 1. Length approximation scheme of the coast line from a polygon with constant modulus segments  $\epsilon$ . (a) Scale =  $\epsilon_0$  and (b) scale =  $\epsilon_1 = \epsilon_0/2$ .

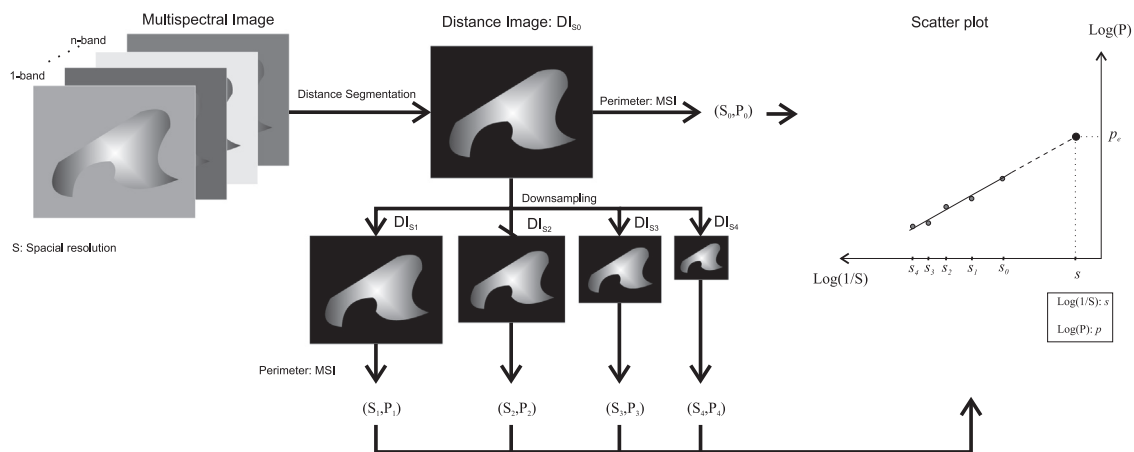


Fig. 2. Complete processing pipeline to perimeter estimation: segmentation + downsampling + measurement + fractal analysis.

### 2.1. Segmentation-classification by minimum distance

The segmentation algorithm is based on the minimum distance concept to one or multiple prototypes (Girard and Girard, 1999; Richards and Jia, 2006). These algorithms permit to build gray-scale images whose threshold improves the use of the available information and enhances the precision of subsequent processing stages (Rivest and Soille, 1995; Sladoje and Lindblad, 2009; Cipolletti et al., 2012).

The chromatic distance establishes a similarity or closeness relation between every pixel in the image and a given prototype. In a multispectral image, a prototype ( $\vec{r}$ ) is a vector whose spectral components offer the best representation of a region from the foreground or background. In this work, each prototype is computed averaging a group of pixels that belongs to different land and water area coverages inside the image.

A distance image (DI) is generated with the distance coefficients  $G$  as a grey scale. Then, the distribution of the  $G$  coefficients determines an optimum threshold value  $U$  to generate a binary or mask image (MI). Pixels with an associated distance above  $U$  are

assumed to belong to the background, and below  $U$  are assumed to belong to the foreground. For instance, the minimum distance criterion classifies every pixel as either foreground or background if the  $G$  operator is closer to the foreground or background prototype, respectively (González and Woods, 1996).

Mono-distance segmentation (Fig. 3a) compares each pixel in the image with only one prototype. A distance function can be established generalizing the generic k-norm operator between vectors:

$$G(i,j) = \sqrt[k]{\sum_{t=1}^n a_t (x_t(i,j) - r_t)^{k_t}} \quad (2)$$

where  $x_t(i,j)$  ( $1 \leq t \leq n$ ) is the pixel in column  $i$  and row  $j$  with its corresponding  $t$ -band information,  $r_t$  ( $1 \leq t \leq n$ ) are the spectral radiance components of the prototype and  $n$  is the total number of information bands or channels that compose the image. This operator weights the difference between the pixel and the prototype in every spectral band raising it to a power  $k_t$  and multiplying it by a factor  $a_t$ . Finally,  $k$  is the k-th root applied over

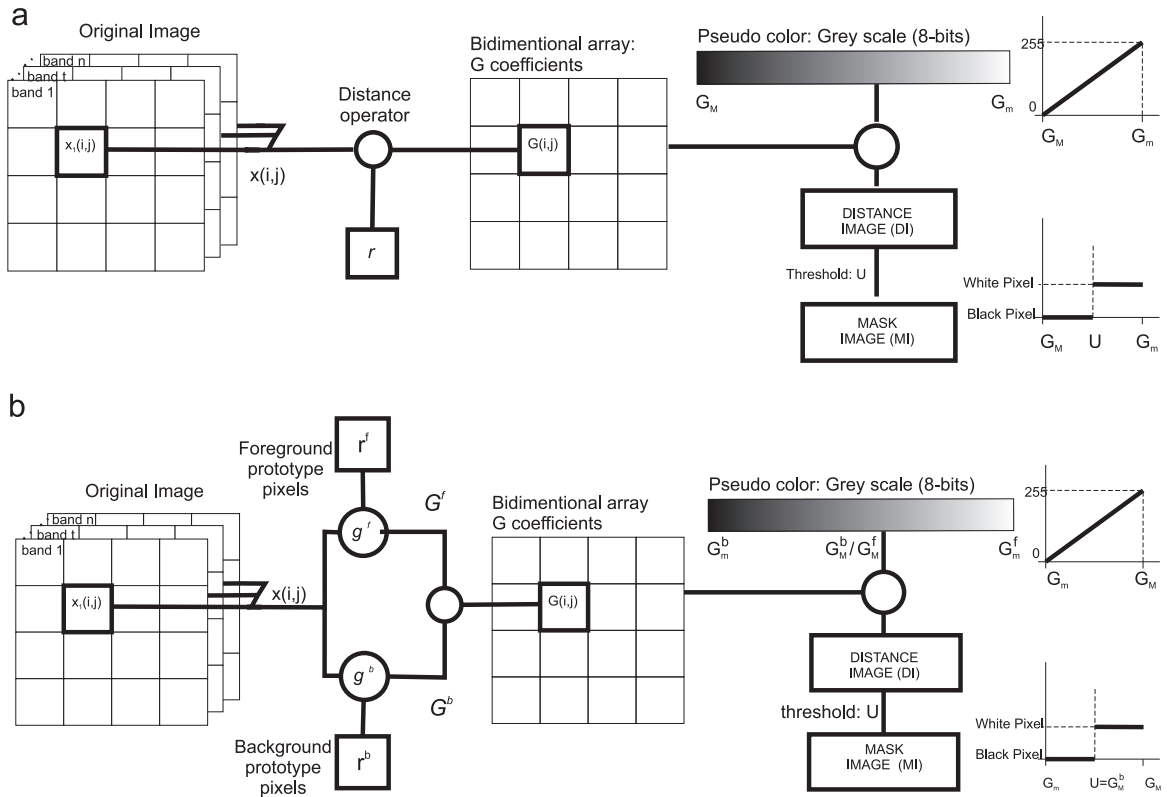


**Fig. 3.** Computing the Distance Image (DI): (a) mono-distance segmentation to only one prototype and (b) multi-distance segmentation to multiple prototypes divided in two representative groups.

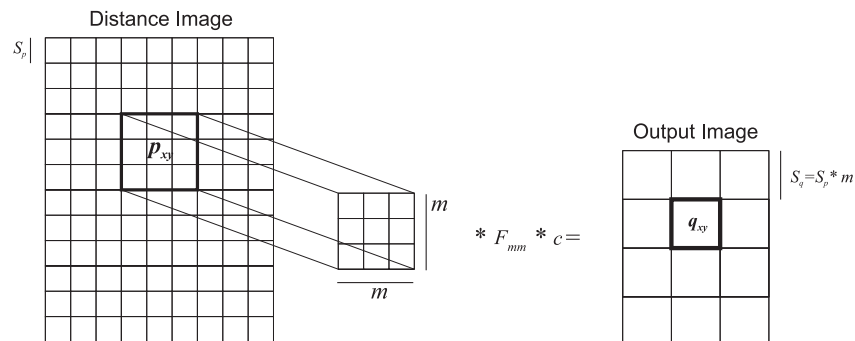


**Fig. 4.** Schematic of the downsampling process.

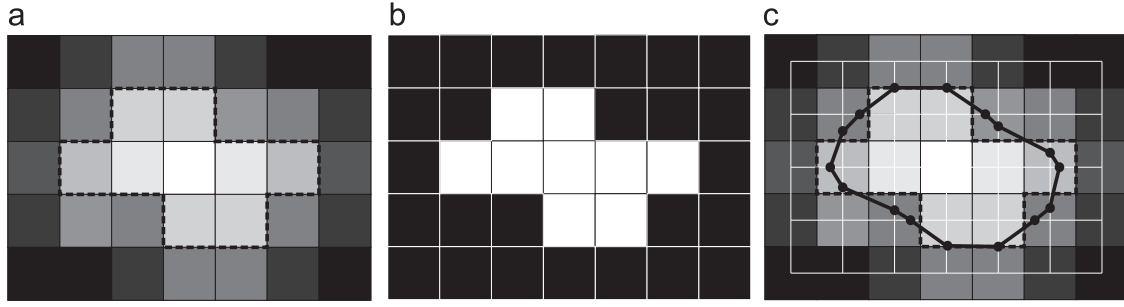


**Fig. 5.** MSI example. (a) Distance image (DI). The black dashed line surrounds the pixels above the threshold. (b) Mask image (MI). (c) Borderline over DI. The white solid line demarcates every Bit Quad (a Bit Quad is a one pixel surface window centered in the middle of  $2 \times 2$  pixels).

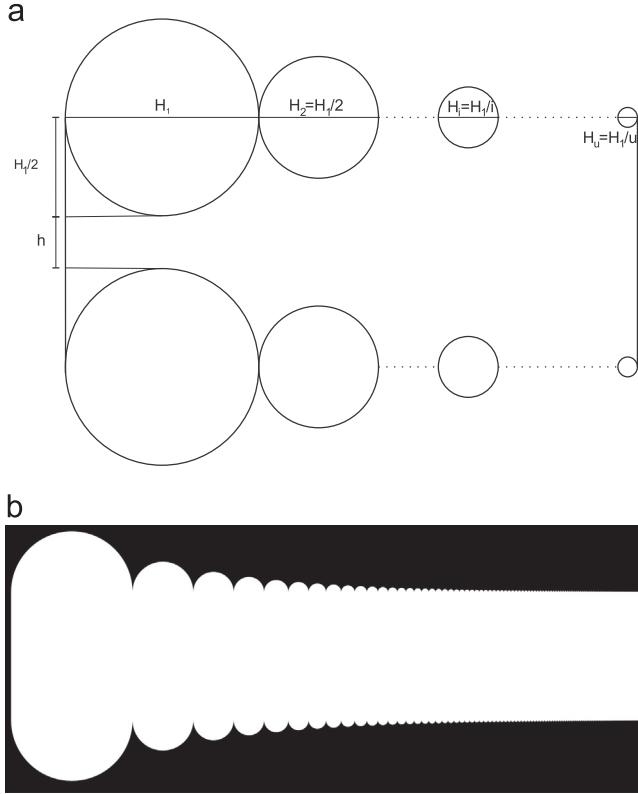


**Fig. 6.** Synthetic island. (a) Construction scheme and (b) resulting image, with spatial resolution  $S = 1$  m.

the summation. This means that  $k=1$  represents Manhattan distance,  $k=2$  Euclid distance and so on. The  $G$  coefficients belongs to the range  $[G_m, G_M]$  where  $G_M$  and  $G_m$  denote the maximum and minimum distance obtained, respectively. The threshold level  $U$  may be established according to several criteria such as Bayesian classifier (Rish, 2001), Otsu method (Otsu, 1979), histogram analysis, etc.

Multi-distance segmentation (Fig. 3b) selects two groups of representative prototypes belonging to each zone:  $r^f$  and  $r^b$ , corresponding to foreground and background, respectively. The superindex  $f/b$  corresponds to the  $f/b$ -th prototype in the foreground/background which ranges between  $1 \leq f \leq F/1 \leq b \leq B$ , where  $F/B$  is the total amount of prototypes of each class. The multi-distance operator is defined as

$$g^f = \sqrt[k]{\sum_{t=1}^n a_t (x_t - r_t^f)^{k_t}},$$

$$G^f = \min_{1 \leq f \leq F} (g^f)$$

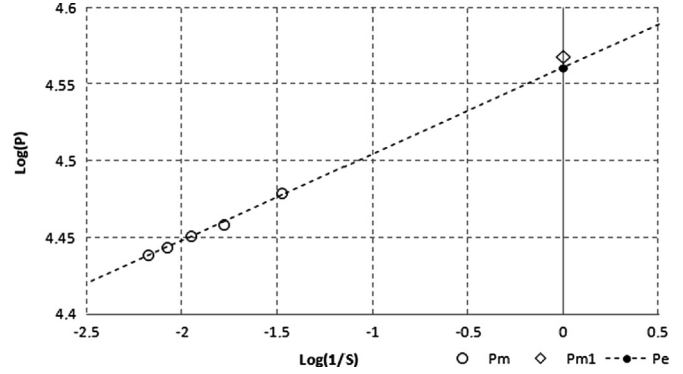


**Fig. 7.** Border length estimation of the synthetic image.

$$g^b = \sqrt[k]{\sum_{t=1}^n a_t (x_t - r_t^b)^{k_t}},$$

$$G^b = \min_{1 \leq b \leq B} (g^b) \quad (3)$$

$$G = \begin{cases} -\frac{G^f}{G^b} & \text{if } G^f \leq G^b \\ \frac{G^b}{G^f} & \text{if } G^f > G^b \end{cases} \quad (4)$$

Given the Eq. (2) with its parameters defined, the distance ( $g^f/g^b$ ) among each pixel in the image and all the reference pixels are calculated, and the minimum corresponding distances obtained are stored ( $G^f/G^b$ ). The final  $G$  pixel coefficient is determined by relating both minimum distances to foreground ( $G^f$ ) and background ( $G^b$ ). In other words, it is calculated as the ratio between  $G^f$  and  $G^b$  if  $G^f \leq G^b$  or  $G^b$  and  $G^f$  if  $G^f > G^b$ . Maximum distance is given by  $G_M = G_M^f - G_m^f + |G_M^b| - |G_m^b|$  and the optimum threshold value is the maximum background distance defined as  $U = |G_M^b|$ .

## 2.2. Downsampling

Downsampling is performed using standard convolution kernels over the DI. A convolution kernel is a matrix of coefficients  $f_{ij}$ . We model the coarser resolution sensor behavior as an uniform sampling of the backscattering function over a given region. For this reason, we apply a kernel of constant coefficients  $c = 1/m^2$  where  $m$  is the desired spatial downsampling factor. In the resulting image, each pixel  $q_{xy}$  is obtained by the convolution product between the kernel and the neighbors pixels to  $p_{xy}$ , normalized by the constant  $c$  (Fig. 4). The downsampling

**Table 1**

Measurement and estimation perimeters for the synthetic island of Fig. 6(b).

$S$ (m)	$P_m$	$\log(S)$	$\log(P_m)$	$P_e$
1	37 047	0	4.568753045	36 439.46
30	30 139.52	1.477121255	4.479136331	30 056.96
60	28 752.44	1.77815125	4.458674706	28 900.29
90	28 257.24	1.954242509	4.45112974	28 244.43
120	27 794.78	2.079181246	4.443963241	27 788.14
150	27 485.81	2.176091259	4.43910854	27 439.29
DF: 1.056614828		$e = 1.64$		$r^2 = 0.9929$

operator is

$$q_{xy} = \left( \sum_{i=1}^m \sum_{j=1}^m f_{ij} p_{ij} \right) * c. \quad (5)$$

### 2.3. Border measurement

The border of the object under study is calculated using the *marching squares with linear interpolation* (MSI) algorithm (Cipolletti et al., 2012). This method tracks the contour using a

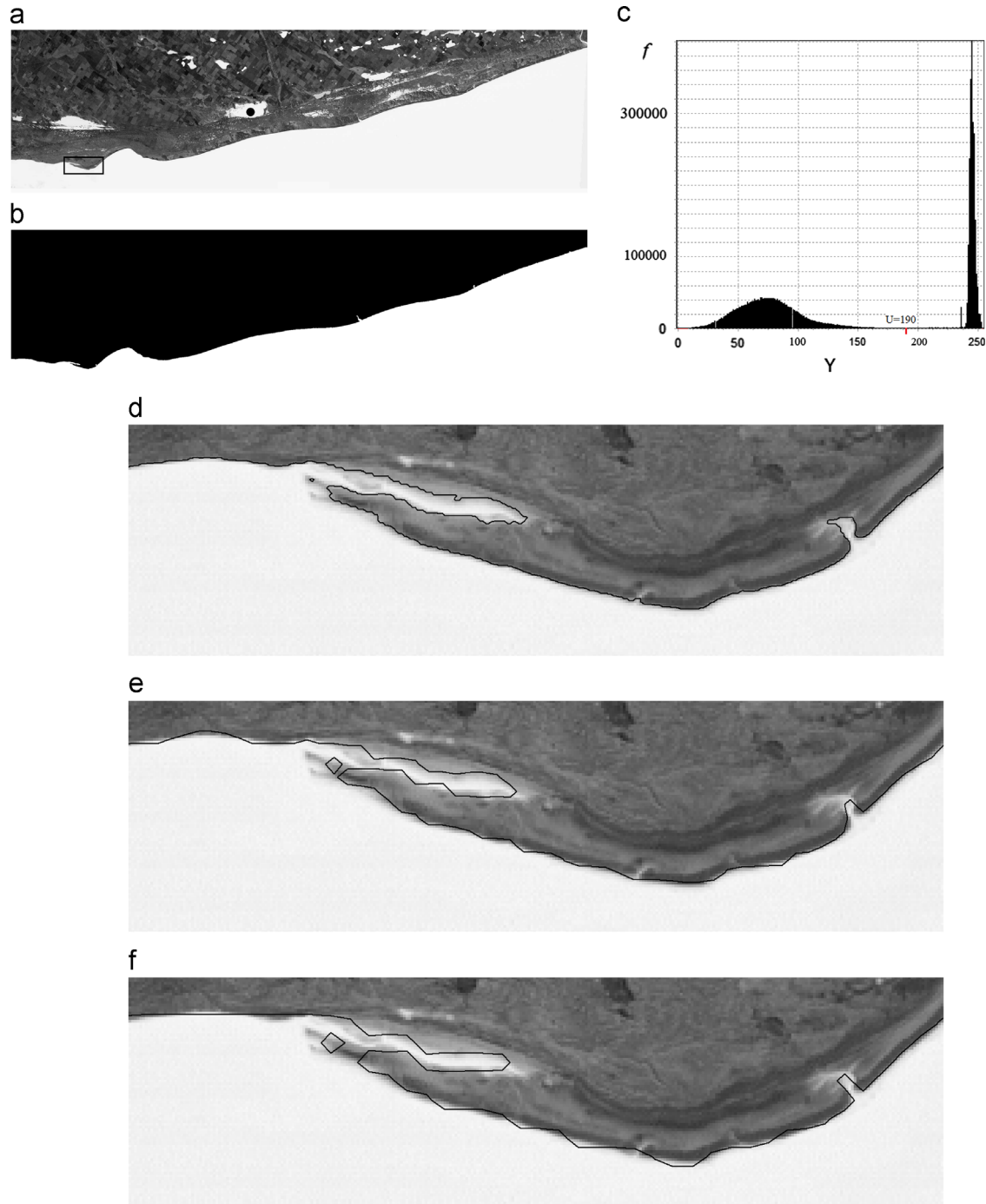


**Fig. 8.** Buenos Aires Province southern coast segmentation and length measurement. (a) Distance image: DI. The black circle area allows to calculate the prototype pixel. (b) Mask image: MI. (c) Distance image histogram. Border coordinates over the original resolution image for a sector calculated with a resolution of: (d)  $S=30$  m. (e)  $S=150$  m. (f)  $S=210$  m.

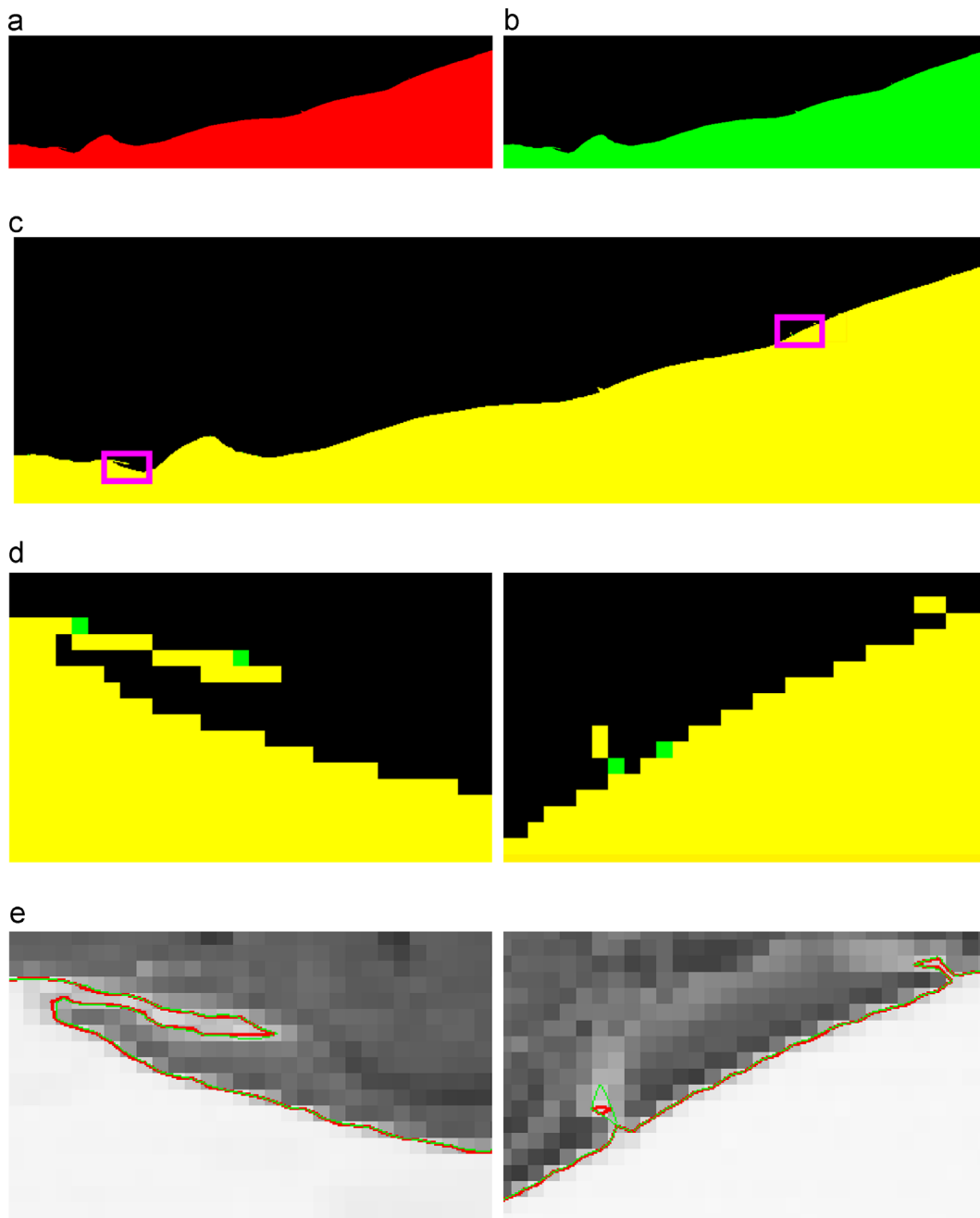


**Fig. 9.** Commutation between segmentation and downsampling. (a) MI: Segmentation + Downsampling. (b) MI: Downsampling + Segmentation. (c) MI superimposition: Fig. 9a and b. (d) Zoom from previous image. (e) Coastline superimposition (in red/green coordinates obtained from MSI method in the  $DI_{(a)}/DI_{(b)}$  image). (For interpretation of the references to color in this figure caption, the reader is referred to the web version of this article.)

super-resolution enhancement of the marching squares or Crack Code algorithm (Dunkelberger and Mitchell, 1985), improving the precision by linear interpolation over distance images.

The border length is approximated by a polygonal with variable length segments capable to adjust the boundaries in any possible orientation (Fig. 5). The algorithm is robust under the geometric and luminance transformations that are usually applied to remote sensing imagery (for instance, rescaling or luminance stretch), and the polygonal border is symmetric with respect to foreground and background (Cipolletti et al., 2012). Although it requires higher computational cost compared to standard methods, the increment in complexity is not significant over the complete processing pipeline.

#### 2.4. Fractal regression

At every downsampling factor  $S$ , a border length  $P(S)$  is measured. The scatter-plot of the  $\log(P(S))$  vs.  $\log(1/S)$  pairs is fitted using standard least squares regression (Gibbs, 2011). The slope of the regressed line is an estimation of the fractal dimension  $D$  of the border under measurement.

With this slope, then, it is possible to predict (i.e., to extrapolate) the border length at any possible scale, with a precision that makes the extrapolated values suitable for geomorphological studies. For this, given the desired scale, the intercept of the regressed line at that scale would be the border length that is numerically congruent with the actual measurements.



### 3. Results

#### 3.1. Validation with synthetic images

The performance of the method is tested with a synthetic image, whose exact border length can be determined mathematically. A binary image of an “island” is generated with known geometric properties. The synthetic resolution of this image is 1 m per pixel ( $S=1$  m).

As shown in Fig. 6a, the “island” is composed by  $u$  semi-circles with diameters between  $H_1 \dots H_i \dots H_u$  where  $H_1 = H_1/1 \dots H_i = H_1/i \dots H_u = H_1/u$ . The side borders are straight lines that tangentially join the upper and lower circles.

The resulting object (Fig. 6b) is composed of  $u=100$  circles in each side, where the largest diameter is  $H_1=2000$  m and the margin is  $h=100$  m. In this way, the figure has a large amount of geometrical features (i.e., curved borders at several curvature radii and orientation) and, therefore, is adequate for testing the whole processing pipeline. The subindexes  $m$ ,  $e$  and  $r$  correspond to the measured, estimated and real values, respectively. The real perimeter is

$$P_r = \pi * \sum_{i=1}^u \frac{H_i}{t} + 2*(H_1 + h) \quad (6)$$

$$P_r = \pi * \sum_{i=1}^{100} \frac{2000}{t} + 2*(2000 + 100) \quad (7)$$

$$P_r = 36\,793.254 \text{ m} \quad (8)$$

Then, the image is downsampled with a downsampling factor 30x, giving a pixel size of 30 m, similar to that of Landsat images. The purpose of this section is to be able to predict the border measurement of the 1 m image using only the 30 m image (this would be equivalent to predict the border length in Ikonos images using Landsat images). For this, the 30 m image is again downsampled 2x, 3x, 4x and 5x (60, 90, 120 and 150 m per pixel, respectively). Over these five images, the border length is measured, the regression on the log–log plot is performed and the border length  $P_{e1}$  at 1 m resolution is estimated.

The accuracy of the method is contrasted with the measured perimeter ( $P_{m1}$ ) in Fig. 6b. The error is calculated as

$$e = \left| 100 * \left( \frac{P_{m1} - P_{e1}}{P_{m1}} \right) \right| \quad (9)$$

where  $P_{e1}$  is the estimated value from the fractal regression for  $S=1$  m.

In Fig. 7, the fractal regression data points are graphically presented and the important points are detailed in Table 1. The error between the measured border in the 1 m image ( $P_{m1}$ ) and the estimated ( $P_e$ ) is lower than 2%, outperforming the standard measurement routines (Kulpa, 1983; Dorst and Smeulders, 1987; Yang et al., 1994; Cipolletti et al., 2012). In addition, the determination coefficient  $r^2$  is almost equal to one, which assures a high correlation between data and estimation. This behavior is also observed in similar synthetic images; therefore, the proposed method for perimeter approximation is reliable within these error levels.

#### 3.2. Validation with Landsat images

The methodology is further tested with Landsat images over a portion of the southern coast of Buenos Aires Province segmented in a Landsat image. The smooth border represents extended segments of the Argentine seaboard, especially the northern part represented by this province. The shoreline border measurement using the original 30 m resolution image (original resolution,

Fig. 8a) is taken as ground truth. A 5x undersampled image (i.e., 150 m per pixel) is employed for border estimation. Over this last image, several undersamplings are performed, the border length is measured, a fractal regression is established and, finally, the fit for the 30 m resolution measurement is extrapolated.

Water segmentation used the 4th, 5th and 7th bands of a Landsat 7 image ( $\vec{x}(i,j) = (B4, B5, B7)$ ). The operator parameters describe an Euclid distance, i.e.,  $\vec{d} = (1, 1, 1)$ ,  $\vec{k} = (2, 2, 2)$  and  $k=2$ . The prototype pixel is computed as a weighted average of a group of pixels from the region marked with a black circle in Fig. 8a. In Fig. 8b, the distribution of the  $G$  values allows to define the threshold value  $U=190$  to generate MI.

In 5x and 8x undersampled images (i.e., 150 and 240 m per pixel, respectively) the reverse process is tested. The original Landsat bands are downsampled and then the segmentation method is applied in order to analyze the difference between the measured perimeters. The image bands and segmentation parameters employed are the same that have previously been established. In the first case, the 5x image presents a 0.4% difference in the measured perimeter and, in the second case, the difference is below 0.1%. Fig. 9 shows the result of overlapping the mask images and polygonal borders obtained for the 5x image.

The measured shoreline length from the  $S=30$  m resolution image is compared with the estimated result by fractal regression. The percent error between the measured ( $P_{m30}$ ) and the estimated ( $P_e$ ) perimeters is lower than 3% and the determination coefficient is  $r^2=0.98$ . Data from the fractal regression and the important points detailed in Table 2 are graphically presented in Fig. 10.

#### 3.3. Validation with high resolution images

Finally, we tested whether the method is able to predict a border measurement over a high resolution satellite image using images of a different, lower resolution satellite mission. For this reason, we analyzed a small island from de Bahía Blanca Estuary in

**Table 2**

Measurement and estimation perimeters for Southern coast of Buenos Aires Province.

$S$ (m)	$P_m$	$\log(P_m)$	$\log(S)$	$\log(P_e)$
30	150 792.54	5.178379865	1.477121255	5.18965968
150	139 494.54	5.144557209	2.176091259	5.14376637
180	137 296.58	5.137659732	2.255272505	5.13856745
210	136 227.39	5.134264398	2.322219295	5.13417182
240	134 692.94	5.129344845	2.380211242	5.13036416
270	134 291.71	5.128049201	2.431363764	5.12700556
DF: 1.06565848				$e\% : 2.56$

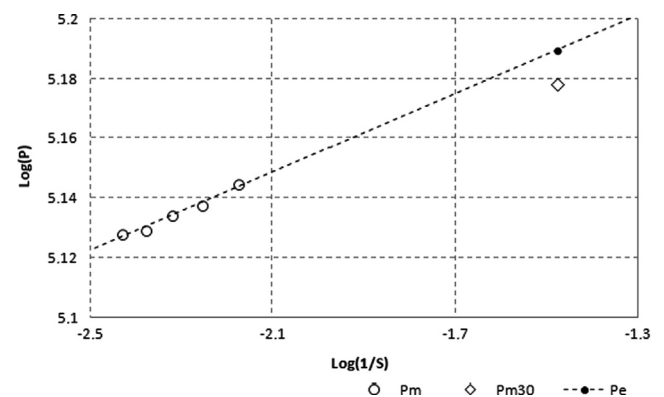


**Fig. 10.** Shoreline length estimation in Landsat image.

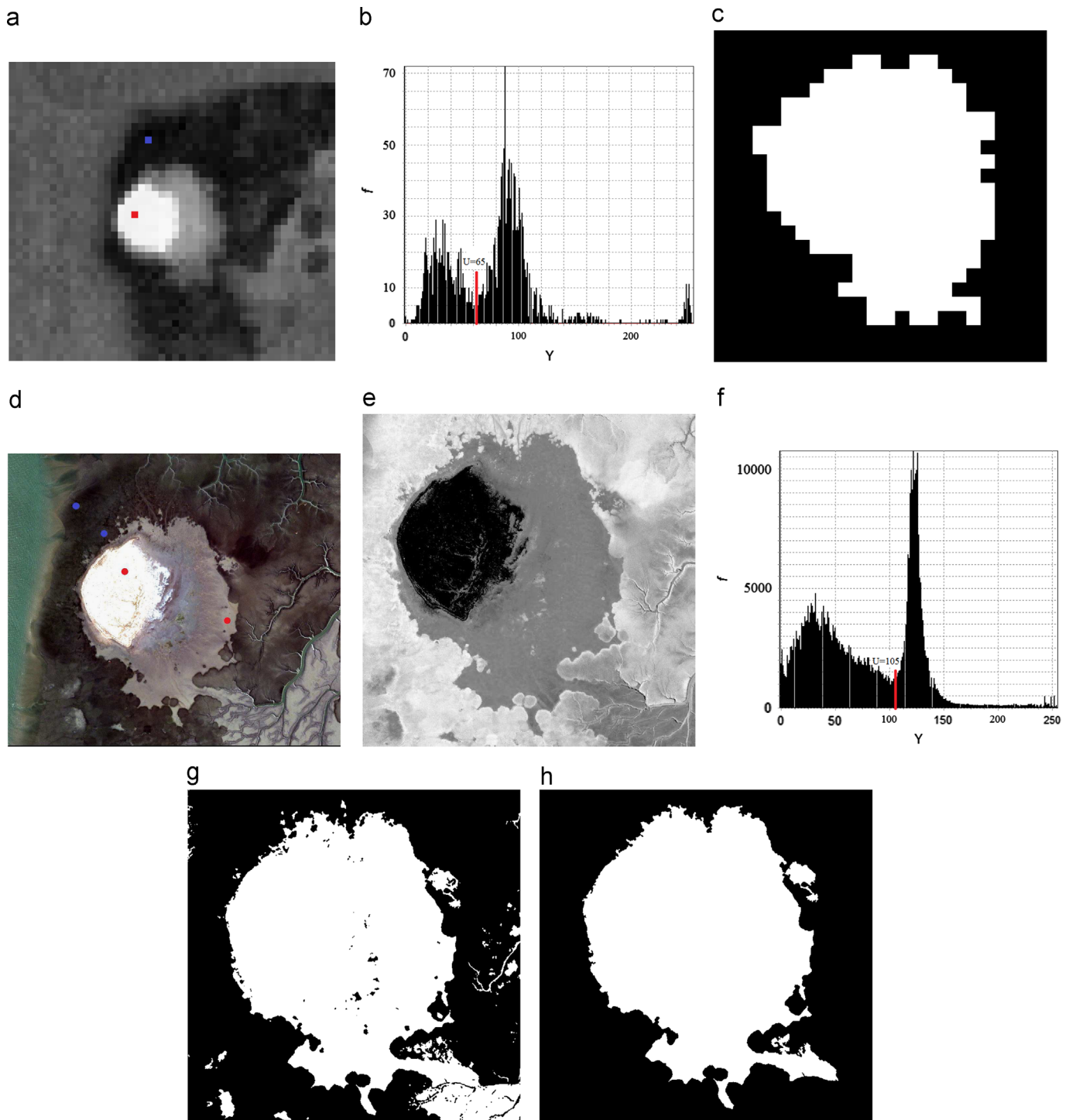


**Fig. 11.** Island in the estuary of Bahía Blanca. Landsat image: (a) DI. (b) DI histogram. (c) Binary image from DI. (d) MI. The foreground/background prototypes pixels are computed as a weighed average from the group of pixels in the regions marked with red/blue circles. (For interpretation of the references to color in this figure caption, the reader is referred to the web version of this article.)

both Ikonos and Landsat images whose high roughness edges present headlands and bays corresponding to most of the Patagonian coast of Argentina and very similar to the British coast employed by Mandelbrot (1967) to make the first fractal analysis of a coastline. The resulting DI (Fig. 11e) produces an inadequate MI (Fig. 11g) and, for this reason, some of the defects are removed by hand to have a clear MI (Fig. 11h).

For the island segmentation, we use bands 1, 2 and 3 of a Landsat 7 image ( $\vec{x}(i,j) = (B1, B2, B3)$ ). In the Ikonos image, the blue, green and red bands are employed ( $\vec{x}(i,j) = (\text{blue}, \text{green}, \text{red})$ ).

In both cases, Euclid distance provides an adequate separation between foreground (land) and background (water) prototypes, (i.e.,  $\vec{a} = (1, 1, 1)$ ,  $\vec{k} = (2, 2, 2)$  and  $k = 2$ ). The foreground and background prototypes are computed as a weighed average from a set of regions selected by hand (red or blue circles in Fig. 11a and d, respectively, within which a Gaussian function is applied for computing the weight of the pixels in their respective prototypes. In Fig. 11b and f we show the distribution of the  $G$  values in both images. Adequate threshold levels to construct MI are  $U = 65$  for the Landsat image and  $U = 105$  for the Ikonos image.



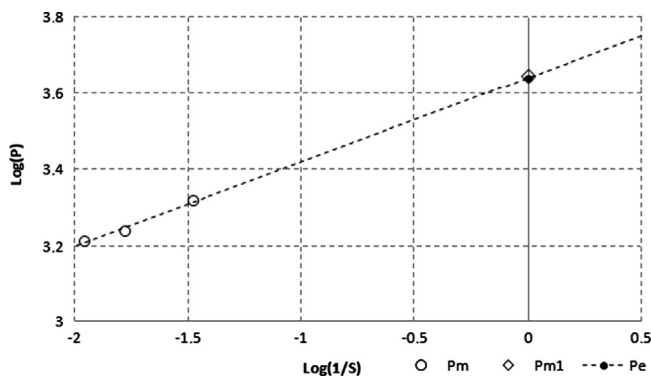
The perimeter  $P_{m1}$  of the island is then measured over this image. Therefore, the same island is segmented in the Landsat image and the perimeter is calculated for several downsamples. In this case, given the small size of the island, only 2x and 3x downsamples are possible (60 and 90 m per pixel, respectively) before the island is unnoticeable in the downsampled image. Even with these very few values, the error between the measured ( $P_{m1}$ ) and the estimated ( $P_e$ ) perimeters is 1.39% and the determination coefficient is  $r^2 \approx 1$ . Fractal regression data and the important points detailed in Table 3 are graphically presented in Fig. 12.

Fig. 13 shows the result of overlapping the mask images and polygonal borders obtained. In each case, Landsat information presents the appropriate change in scale. Even if the Landsat image does not have the high frequency details present in the Ikonos image, their correspondence is clear.

**Table 3**

Measurement and estimation perimeters for a small island belonging to the Bahía Blanca Estuary.

S (m)	$P_m$	$\log(P)$	$\log(S)$	$\log(P_e)$
1	4451.42	3.64849857		3.642437745
30	2086.03	3.31932055	1.47712125	3.316553686
60	1748.41	3.24264328	1.77815125	3.250140129
90	1644.45	3.21602067	1.95424250	3.211290689
DF: 1.220621061				$e_{\%} : 1.39$



**Fig. 12.** Perimeter estimation of a small island in the Bahía Blanca Estuary.

#### 4. Discussion

The associated error is low and it does not increase for higher roughness levels. The method has been tested for several image modalities and, in all cases, the error obtained is lower than 5%, improving the performance of classic measurement algorithms in direct measurement conditions. In each case, the determination coefficient  $r^2$  is almost equal to one, assuring a high correlation. Whereas the coast of Buenos Aires Province presents a smooth roughness which is reflected in its FD (1.07), the FD obtained for the island is 1.22, similar to the FD of the west coast of Britain (Mandelbrot, 1967), considered one of the roughest coasts worldwide.

As opposed to the method presented in Håkanson (1978), our method has homogeneous information and establishes an initial condition over the initial resolution image, avoiding the use of heterogeneous cartography. Once the segmentation process and the threshold selection are completed, pixels from foreground and background are univocally determined. The DI remains constant and is used to construct the coarse spatial resolution DIs.

Since the segmentation is performed only once, the computational cost is thus considerably reduced while the difference between measurements on the perimeter is negligible. The presence of spurious pixels in the original DI are minimized during the downsampling process, given the fact that coarse resolution pixels are a composition of themselves and their neighbors.

Although the method has been tested over coastline segments, its application is possible on any topographic contours with auto-similarity patterns (such as coastlines, tidal channels, river basin, etc.). For example, Rodríguez-Iturbe and Rinaldo (1997) claim that the contour lines on a topographic map of a river basin are analogous to the coastlines studied. When the linear geographic feature under measure exhibits non-fractal behavior (i.e., has an integer fractal dimension, see Wolinsky et al., 2010 for a particular geomorphology where this happens) then its behavior is classical isometric and, therefore, our regression will measure consistently the same length  $L$  at all scales, which confirms that the extrapolated values are also highly reliable.

#### 5. Conclusions

A perimeter estimation method is proposed based on fractal extrapolation. This estimation predicts the value of a measurement

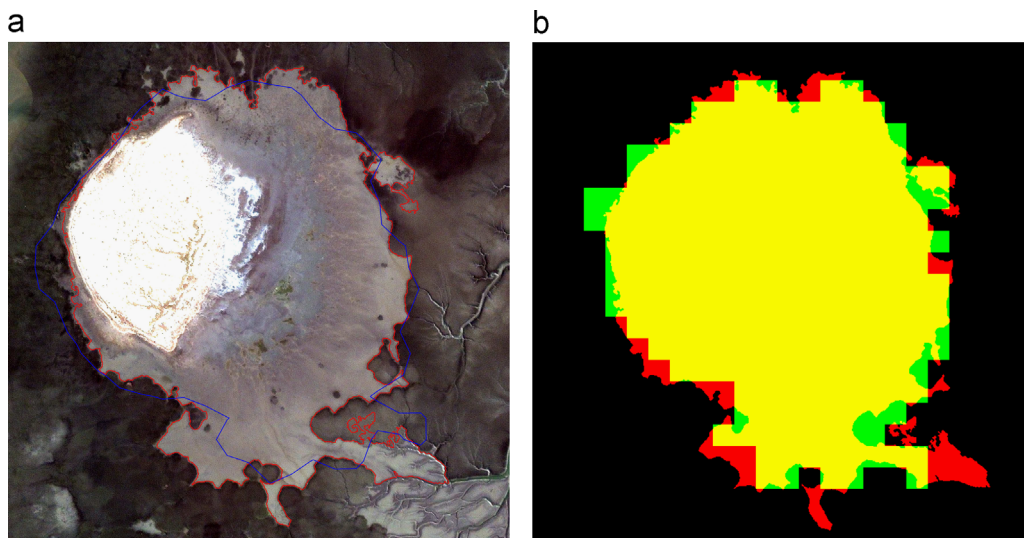


**Fig. 13.** Superimposition results. (a) Coastline superimposition (in red/blue coordinates obtained from MSI method in the Ikonos/Landsat image). (b) MI superimposition. (For interpretation of the references to color in this figure caption, the reader is referred to the web version of this article.)

performed in a scale much more detailed than the original available and avoids information incongruence problems due to the use of heterogeneous cartography. The algorithm establishes the fractal regression that relates measurements taken at different resolutions and employs this information to extrapolate the value corresponding to an hypothetic measurement taken with a much higher resolution. The extrapolation results are shown to be very precise both, in synthetic images (of controlled resolution) and in geographic areas for which satellite images of different resolutions (Landsat and Ikonos) were available. The first tests were performed on sectors from the coast of the Buenos Aires Province and were continued on a small island in the Bahía Blanca Estuary.

Given the promising preliminary results obtained, it is expected to use this extrapolation technique in larger geographic areas, such as the complete coastline of Argentina or the study of tidal channel and river plain view geomorphology as suggested by Angeles et al. (2004) and Snow (1989), respectively.

## Acknowledgments

Partial support for this study has been provided by Grants from CONICET, ANPCYT and UNS through projects under the direction of C.A. Delrieux, G.M.E. Perillo and M.C. Piccolo. The authors wish to thank two anonymous reviewers for their constructive comments.

## References

- Allen, M., Brown, G., Miles, N., 1995. Measurement of boundary fractal dimensions: review of current techniques. *Powder Technology* 84 (1), 1–14.
- Angeles, G., Perillo, G.M.E., Piccolo, M.C., Pierini, J., 2004. Fractal analysis of tidal channels in the Bahía Blanca estuary (Argentina). *Geomorphology* 57 (3–4), 263–274.
- Chen, C., Ho, P.-G.P., 2008. Statistical pattern recognition in remote sensing. *Pattern Recognition* 41 (9), 2731–2741.
- Cipolletti, M.P., Delrieux, C.A., Perillo, G.M.E., Piccolo, M.C., 2012. Superresolution border segmentation and measurement in remote sensing images. *Computers and Geosciences* 40 (0), 87–96.
- Dillon, C., Carey, P., Worden, R., 2001. Fractscript: a macro for calculating the fractal dimension of object perimeters in images of multiple objects. *Computers and Geosciences* 27, 787–794.
- Dorst, L., Smeulders, A.W., 1987. Length estimators for digitized contours. *Computer Vision, Graphics, and Image Processing* 40 (3), 311–333.
- Dunkelberger, K., Mitchell, O., 1985. Contour tracing for precision measurement. In: *Proceedings of the International Conference on Robotics and Automation*, vol. 2, IEEE, West Lafayette, Indiana, pp. 22–27.
- Dutch, S., 1993. Linear richardson plots from non-fractal data sets. *Mathematical Geology* 25 (6), 737–751.
- Falconer, K., 2003. *Fractal Geometry: Mathematical Foundations and Applications*. Wiley, England.
- Freeman, H., 1961. On the encoding of arbitrary geometric configurations. *IEEE Transactions on Electronic Computers* 10 (2), 260–268.
- Freeman, H., 1970. Boundary encoding and processing. In: Lipkin, B.S., Rosenfeld, A. (Eds.), *Picture Processing and Psychopictics*, New York. Symposium on Psychopictics held at Arlington, pp. 241–263.
- García, J.V., Oleschko, K., noz Villalobos, J.M., Velásquez-Valle, M., Menes, M.M., Parrot, J., Korvin, G., Cerca, M., 2010. Land cover monitoring by fractal analysis of digital images. *Complexity and Nonlinearity in Soils* 160, 83–92.
- Gibbs, B., 2011. *Advanced Kalman Filtering, Least-Squares and Modeling*. John Wiley & Sons, New Jersey.
- Girard, C.M., Girard, M.C., 1999. *Processing of Remote Sensing Data*. Dunod, Paris.
- González, R., Woods, R., 1996. *Digital Image Processing*. Addison-Wesley, Wilmington, DE.
- Goodchild, M.F., 1980. Fractals and the accuracy of geographical measures. *Mathematical Geology* 12 (2), 85–98.
- Håkanson, L., 1978. The length of closed geomorphic lines. *Mathematical Geology* 10 (2), 141–167.
- Imre, A., 2006. Artificial fractal dimension obtained by using perimeter–area relationship on digitalized images. *Applied Mathematics and Computation* 173, 443–449.
- Imre, A., Cseh, D., Neteler, M., Rocchini, D., 2011. Korcak dimension as a novel indicator of landscape fragmentation and re-forestation. *Ecological Indicators* 11 (5), 1134–1138.
- Korčák, J., 1938. Deux Types Fondamentaux de Distribution Statistique. XXIVe session de l'Institut International de Statistique. Comité D'Organisation.
- Kulpa, Z., 1983. More about areas and perimeters of quantized objects. *Computer Vision, Graphics and Image Processing* 22 (2), 268–276.
- Lam, N.N., Quattrochi, D., 1992. On the issues of scale, resolution, and fractal analysis in the mapping sciences. *Professional Geographer* 44 (1), 88–98.
- Lillesand, T., Kiefer, R., 2000. *Remote Sensing and Image Interpretation*, 4th edition. Wiley & Sons, New York.
- Lipiec, J., Hatano, R., Słowińska-Jurkiewicz, A., 1998. The fractal dimension of pore distribution patterns in variously-compacted soil. *Soil and Tillage Research* 47 (1–2), 61–66.
- Lopes, R., Betrouni, N., 2009. Fractal and multifractal analysis: a review. *Medical Image Analysis* 13, 634–649.
- Mandelbrot, B., 1967. How long is the coast of Britain? Statistical self-similarity and fractional dimension. *Science* 156 (3775), 636–638.
- Mandelbrot, B., 1983. *The Fractal Geometry of Nature*. W.H. Freeman, New York.
- Mark, D.M., Aronson, P.B., 1984. Scale-dependent fractal dimensions of topographic surfaces: an empirical investigation, with applications in geomorphology and computer mapping. *Mathematical Geology* 16 (7), 671–683.
- Otsu, N., 1979. A threshold selection method from gray-level histograms. *IEEE Transactions on Systems, Man and Cybernetics* 9 (1), 62–66.
- Richards, J.A., Jia, X., 2006. *Remote Sensing Digital Image Analysis: An Introduction*. Springer, Berlin.
- Richardson, L., 1961. The problem of contiguity: an appendix of statistics of deadly quarrels. *General Systems Yearbook of the International Society for Science* 6, 139–187.
- Rish, I., 2001. An Empirical Study of the Naive Bayes Classifier. Technical Report, IBM Research Division.
- Rivest, J.-F., Soille, P., 1995. Physical significance of image measurements. *IEEE Transactions on Instrumentation and Measurement* 44 (3), 751–754.
- Rodríguez-Iturbe, I., Rinaldo, A., 1997. *Fractal River Basins*. Cambridge University Press, United Kingdom.
- Russ, J.C., 1993. *Fractal Images*. Plenum Press.
- Schlueter, E., Zimmerman, R., Witherspoon, P., Cook, N., 1997. The fractal dimension of pores in sedimentary rocks and its influence on permeability. *Engineering Geology* 48, 199–215.
- Schowengerdt, R., 1997. *Remote Sensing Models and Methods for Image Processing*, 2th edition Academic Press, San Diego.
- Shelberg, M., Moellerling, H., Lam, N., 1982. Measuring the fractal dimensions of empirical cartographic curves. In: *Proceedings of the International Symposium on Computer Cartography*, pp. 481–490.
- Siu, N., Lam, N., 2002. *Fractals in Geography*. The Blackburn Press, U.S.A. ISBN: 1-930665-69-5.
- Sladoje, N., Lindblad, J., 2009. High-precision boundary length estimation by utilizing gray-level information. *IEEE Transactions on Pattern Analysis and Machine Intelligence* 31 (2), 357–363.
- Snow, R., 1989. Fractal sinuosity of stream channels. *Channels* 131 (1–2), 99–109.
- Soille, P., Rivest, J.-F., 1996. On the validity of fractal dimension measurements in image analysis. *Journal of Visual Communication and Image Representation* 7 (3), 217–229.
- Wolinsky, M., Edmonds, D., Martin, J., Paola, C., 2010. Delta allometry: growth laws for river deltas. *Geophysical Research Letters* 37, L21430.
- Wu, J., 2004. Effects of changing scale on landscape pattern analysis: scaling relations. *Landscape Ecology* 19, 125–138. <http://dx.doi.org/10.1023/B:LAND.0000021711.40074.ae>.
- Wu, J., Li, H., Jones, K., Loucks, O., 2006. Scaling with known uncertainty: a synthesis. In: Wu, J., Jones, K., Li, H., Loucks, O. (Eds.), *Scaling and Uncertainty Analysis in Ecology*. Springer, Netherlands, pp. 329–346. 10.1007/1-4020-4663-4\_18.
- Yang, L., Albregtsen, F., Lønnestad, T., Grøttum, P., 1994. Methods to estimate areas and perimeters of blob-like objects: a comparison. In: *Proceedings of the IAPR Workshop on Machine Vision Applications*. Kawasaki, MVA, pp. 272–276.
- Zhende, H., Yuwen, Q., 2003. The study of fractal correlation method in the displacement measurement and its application. *Optics and Lasers in Engineering* 39, 465–472.
- Zuo, R., Agterberg, F., Cheng, Q., Yao, L., 2009. Fractal characterization of the spatial distribution of geological point processes. *International Journal of Applied Earth Observation and Geoinformation* 11 (6), 394–402.